Early hydration of ye'elimite: insights from thermodynamic modelling

Maciej Zajac[1], Jan Skocek[1], Frank Bullerjahn[1], Barbara Lothenbach[2], Karen Scrivener[3], Mohsen Ben Haha[1]

[1] Global R&D HeidelbergCement AG, Oberklamweg 2-4, 69181 Leimen, Germany

[2] Empa, Swiss Federal Laboratories for Materials Science and Technology, Laboratory for Concrete/Construction Chemistry, Überlandstrasse 129, 8600 Dübendorf, Switzerland

[3] EPFL STI IMX LMC MXG 232 (Bâtiment MXG) Station 12 CH-1015 Lausanne Switzerland

1   **Abstract**

2   This study focuses on better understanding of early reaction of ye'elimite, the main constituent of calcium

3   sulfoaluminate cements and the effect of minor phases.

4   Thermodynamic modelling was used to calculate the solubility in the tri-dimensional space of Ca-Al-S-H$_2$O at

5   different alkali concentrations and compared to changes in the pore solution concentrations during the

6   ye'elimite reaction. It is demonstrated that the hydration pathways follow the stability fields of certain

7   hydrates. The interplay between the solution properties and the solubility of different phases results in an

8   increase of aluminium, sulfate, and calcium concentrations following the congruent dissolution of ye'elimite.

9   Moreover, once hydrates start to precipitate, their supersaturation does not change as intensely as the pore

10   solution concentration. This explains the slow reaction of pure ye'elimite. The same framework was applied

11   to explain fast reaction of ye'elimite in the industrial clinkers and particularly the effect of C$_{12}$A$_7$ and alkalis.

12
13   Key words

14   A Hydration, A Reaction, B Thermodynamic Calculations, B Pore Solution, D Sulfoaluminate, E Modelling

15   **1.   Introduction**

16   Ye'elimite phase is an important component of calcium sulfoaluminate (CSA) cements. CSA cement has been

17   used in China as the "third cement series" for more than 30 years for construction and special applications

18   [1] [2] and today, the production of CSA cement in China is more than 1 million tonnes per year [3]. Recently,

19   belite-rich CSA cements, so-called belite ye'elimite ferrite (BYF) cements are gaining increasing attention of

20   cement producers [4][5][6] as a low CO$_2$ alternative to Portland cement. Despite the long history of the CSA

21   systems use in many applications, the early hydration mechanisms of ye'elimite clinkers and/or cements are

22   not well understood although the understanding of this mechanisms is very important since the hydration of

23   ye'elimite regulates the evolution of the early cement performance [2] [7].

24   With water alone, the hydration of ye'elimite is often idealized according to the simple equation:

$$1\ C_4A_3\overline{S} + 18\ H \rightarrow 1\ C_4A\overline{S}H_{12} + 2\ AH_3 \text{ Equation 1}$$

25   to form monosulfate and aluminum hydroxide, with the latter being usually X-ray amorphous. The addition

26   of anhydrite modifies the reaction to:

$$1\ C_4A_3\overline{S} + 2\ C\overline{S} + 38\ H \rightarrow 1\ C_6A\overline{S}_3H_{32} + 2\ AH_3 \text{ Equation 2}$$
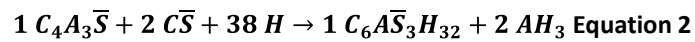
27   According to these reactions, the reaction products are monosulfate or ettringite and aluminium hydroxide

28   in the final product. The content of ettringite and monosulfate is regulated by the ratio between ye'elimite

29   and calcium sulfate. However, many publications [2] [8] [9][10] suggested that the reaction of ye'elimite with

30   water is more complex than these simplified reactions as summarised in. The products of the synthetic

31   ye'elimite reaction include a substantial amount of amorphous CAH_{10} phase and ettringite in addition to

32   aluminium hydroxide and monosulfate [9][10]. The formation of CAH_{10} has also been observed in hydrated

33   industrial clinkers and cements [11] [12] [13][14]. The CAH_{10} phase precipitation is closely linked to the nature

34   of aluminium hydroxide. Aluminium hydroxide has three forms: XRD amorphous, microcrystalline phase or

35   crystalline gibbsite [15] [16] [17]. These forms are characterized by different solubilities, amorphous

36   aluminium hydroxide is the most soluble while gibbsite has the lowest solubility but it generally forms very

37   slowly at room temperature [18]. During the early hydration, the amorphous form of aluminium hydroxide

38   precipitates which stabilizes the CAH_{10} phase [11] [18] [8]. Later on, when microcrystalline aluminium

39   hydroxide forms, the CAH_{10} phase is destabilized. Hence, even the hydration of the neat ye'elimite phase is

40   more complex than the idealized reactions (1) and (2). Furthermore, the kinetics of the ye'elimite reaction

41   vary strongly depending on the system investigated. Synthetic, pure ye'elimite reacts slowly [2][9] [19] while

42   ye'elimite in industrial cements may react very rapidly [1] [8][20] [21] [22].

43   Despite considerable research on ye'limite / CSA hydration, there are few reported studies linking the pore

44   solution properties with the evolution of the solid phases. Such studies are needed for understanding the

45   early hydration mechanisms. Additionally, many of the studies focusing on early hydration investigated

46   cement clinker or cements and using retarders [20] [23] [24], which may interfere with the hydration of the

47   ye'elimite. Consequently, this hinders understanding the mechanisms of early reactions. Additionally, the

48   earliest pore solution extractions reported are too late [20] [25] [26] [19] to capture all the early hydration

49   features as these are typically gained only after few hours after the mixing with water.

50   The two main process that governs the hydration phenomena are dissolution and precipitation [28]. A

51   suitable way to investigate the mechanisms of hydration is to compare the evolution of the pore solution

52   composition resulting from the dissolution of anhydrous phases with the solubility surfaces of hydrates that

53   may precipitate [28] [29]. In this paper, The GEM-Selektor software was applied to investigate the stability

54   of hydrates in the $Ca-Al-S-K-H_2O$ system. The solubility surfaces for the main hydrates which may precipitate

55   during the reaction of ye'elimite were calculated and compared them to the solution data to investigate the

56   mechanisms of ye'elimite hydration, depending on the Ca, Al, S and alkali concentrations in the solution.

57   The thermodynamic modelling of the system $Ca-Al-S-H_2O$ and its sub-systems have been previously

58   investigated by Damidot and Glasser using the state of the art databases available at that time [30] [31] [32].

59   However, the pore solution was treated in a simplified form without considering ion speciation. This is an

60   important aspect since the measured data on the Al, Ca and S concentration vary between µM and hundreds

61   of mM during the hydration of ye'elimite. Additionally, the alkali concentration is typically limited to 0.1 - 1

62   mM in the synthetic systems but can be hundreds of mM in the industrial cements [25]. The use of a modern

63   geochemical software package, GEM-Selector, together with its standard database [33] [34] allows

64   calculation of aqueous ion activities and speciation for the particular system studied. This thermodynamic

65   database has been extended and updated considerably, as summarised in [11][18][35][36] allowing the state-

66   of-the-art modelling.

67   In the present work, the starting point is the simple and relatively well known system $Ca-Al-H_2O$. It is analysed

68   to explain the early hydration of calcium aluminate cements. In the next sections, more complex systems are

69   presented including gradually the effect of alkalis and sulphate on the $Ca-Al-H_2O$ system. Finally, the Ca-Al-S-

70    $K-H_2O$ system is discussed from the perspective of the reaction of the pure ye'elimite and ye'elimite in a

71   cement clinker in order to consolidate our knowledge on the early hydration of the calcium sulfoaluminate

72   phase.

73   **2.   Materials and methods**

74   **2.1. Thermodynamic modelling**

75   Thermodynamic modelling was carried out using the geochemical modelling program GEM-Selector version

76   3.2 [37] [38] with thermodynamic data from the PSI-GEMS database [33] [34] supplemented by cement

77   specific data from the CEMDATA18 database [35][36]. The database compiles thermodynamic data for

78   hydrates such as ettringite, monosulfate and CAH_{10}. The thermodynamic database includes also data for

79   amorphous aluminium hydroxide ($Al(OH)_3$(am), log K_{S0} = 0.24 for the reaction $Al(OH)_3$(am) + OH^- ⇔ $Al(OH)_4^-$

80   [18]), which has a higher solubility than microcrystalline aluminium hydroxide ($Al(OH)_3$(mic), log K_{S0} = - 0.67

81   for the reaction $Al(OH)_3$(mic) + OH^- ⇔ $Al(OH)_4$; [35]. The CEMDATA18 database was completed with

82   thermodynamic data for the solubility of ye'elimite from [39] ($\Delta G°_f$ = -7929.5 kJ/mol for $Ca_4(Al_6O_{12})SO_4$).

83   GEM-Selector is a broad-purpose geochemical modelling code which computes equilibrium phase

84   assemblage and speciation in a complex chemical system from its total bulk elemental composition. The

85   activity of a species i, $\{i\}$, is calculated with GEM-Selector from the measured concentrations in mol/kg H_2O,

86   m_i, considering the formation of aqueous complexes as $\{i\} = m_i\gamma_i$, where γ_i is the dimensionless activity

87   coefficient. The activity coefficients of the aqueous species γ_i were computed with the built-in extended

88   Debye-Hückel equation with common ion-size parameter a_i of 3.67 Å for KOH solutions and common third

89   parameter b_y according to Equation 3:

90    $$\log \gamma_i = \frac{-A_y z_i^2 \sqrt{I}}{1 + B_y a_i \sqrt{I}} + b_y I \quad \text{Equation 3}$$

91   where z_i denotes the charge of species i, I the effective molal ionic strength in mol/kg H_2O, b_y is a semi-

92   empirical parameter (～0.123 kg H_2O/mol for KOH electrolyte at 25°C), and A_y and B_y are P,T-dependent

93   coefficients; at 25°C and 1 bar pressure, A_y ≈ 0.5114 and B_y ≈ 0.3288. This activity correction is applicable up

94   to approx. 1 M ionic strength.

2.2. Solubility curves and surfaces

This thermodynamic data were used to calculate the solubility of different hydrates under equilibrium conditions as a function of calcium, aluminium, sulphur and potassium concentrations within the system Ca-Al-S-K-H_2O and plotted as lines in 2-dimensional and as surfaces in 3-dimensional plots within the concentration range 0.01 mM to 100 mM. The K^+ concentration was varied from 1 to 200 mM to assess the effect of pH. The hydrates considered include hemihydrate, gypsum, portlandite, monosulfate, CAH_{10}, $C_2AH_{7.5}$, C_4AH_{13}, C_3AH_6, gibbsite and amorphous as well as microcrystalline aluminium hydroxide. The limited number of the phases considered was to facilitate and accelerate the calculations. The selection of phases included into the calculations has no impact on the results as interactions neither among the phases nor between phases and the solution were considered.

The solubility line or surface for a given phase corresponds to the concentrations at saturation (saturation index SI is 0). The saturation index is defined as:

$$SI = \log\left(\frac{IAP}{K_{sp}}\right) \quad \text{Equation 4}$$

where IAP is the ion activity product, i.e. the concentrations of the involved species in the investigated space and K_{sp} is the solubility of the given phase. If the SI is higher than 0, i.e. above the line or surface, the solution is oversaturated, below it (SI < 0) is undersaturated with respect to that specific phase. The undersaturation with respect to the dissolving ye'elimite was calculated as well. However, the solubility of the ye'elimite was decreases by 20 log units to make plotting of its solubility line into graphs with the hydrated phases possible. This was needed since the solubility of ye'elimite is significantly higher than the ones of hydrates. The reduced solubility line is market as Y-20 in graphs.

2.3. Pore solution data

Finally, the calculated solubility curves and surfaces were compared with the available experimental data on the pore solution concentrations. This enables the kinetic path of the early reaction of ye'elimite to be tracked as well as the path through the solubility curves and surfaces of the hydrates based on the evolution

119 of the pore solution. For the reaction of the pure ye'elimite early age solution data published in [9] were

120 used, where the ye'elimite hydration was investigated at w/b = 100 and 40 allowing the solution

121 concentrations to be followed during the early reaction. For the reactions occurring in cement clinkers, the

122 pore solution data from Zajac et al. [20] were used, where an industrial BYF clinker had been studied. The

123 clinker contained belite, ye'elimite and ferrite phase as the main components. In the industrial clinkers

124 ye'elimite reacts first, while the hydration of belite and ferrite phases occurs only after days of hydration [20]

125 [21] [40].

126 **3. Results and discussion**

127 **3.1. Solubility lines in Ca-Al-H2O system**

128 The solubility curves of the hydrated phases in the Ca–Al–H_2O and the Ca–Si–H_2O systems have been used to

129 interpret the hydration of the calcium alumina and calcium silicate phases, respectively [41] [28]. The

130 solubility diagram of Ca–Al–H_2O has been used to explain the early hydration of the calcium alumina cement

131 (CAC), and particularly the effect of $C_{12}A_7$ on the acceleration of the hydration of the CA phase and on the

132 resulting phase assemblage [42] [43]. Upon contact with water, the CA phase from CAC dissolves and the

133 solution concentrations increase with a Ca/Al = 0.5 (as indicated by the dotted CA line in Figure 1). The

134 solution is always supersaturated with respect to aluminium hydroxide as soon as CA starts to dissolve. With

135 ongoing dissolution highlighted by the dotted line, the solution intersects the solubility line of CAH_{10} phase

136 as shown in Figure 1. However, the slow nucleation of CAH_{10} and aluminium hydroxide results in a long

137 induction period of the CAC. The presence of small amounts of $C_{12}A_7$ phase increases the Ca/Al, such that the

138 solution crosses earlier the solubility curve of $C_2AH_{7.5}$ which nucleates and precipitates rapidly, shortening

139 the setting time of the cement.

140

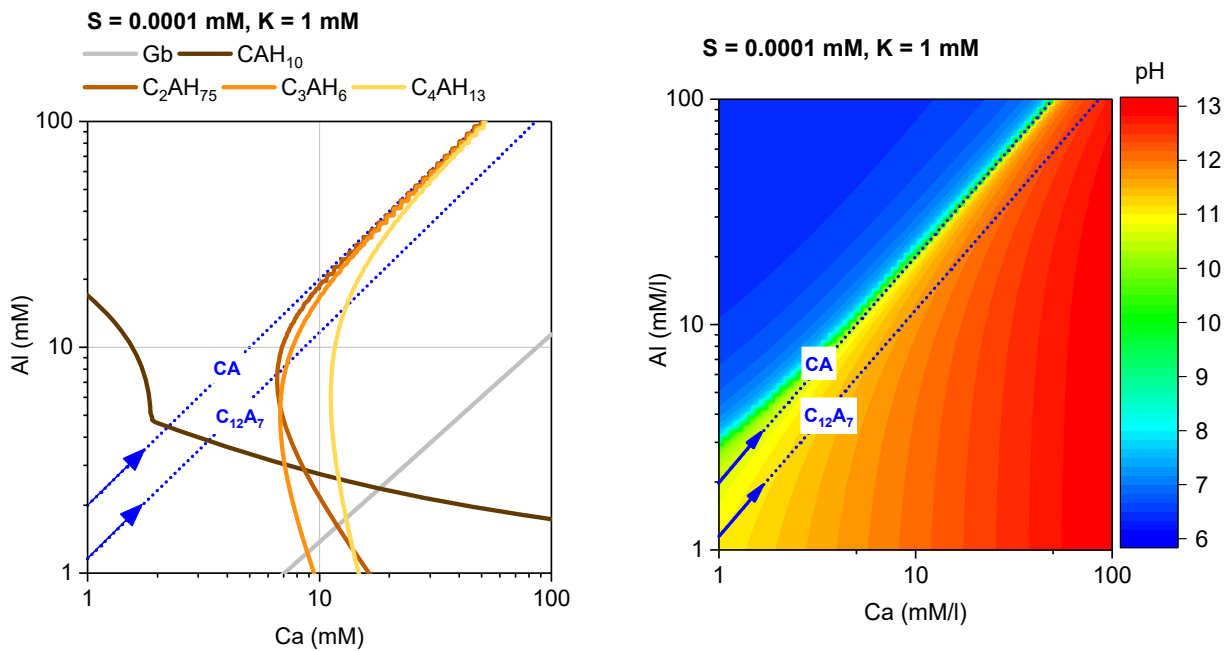**S = 0.0001 mM, K = 1 mM**

S = 0.0001 mM, K = 1 mM

Figure 1 Left: Solubility lines for the relevant hydrates formed during the hydration of CAC, Gb – gibbsite. Below the lines the respective solid is undersaturated and cannot precipitate. Increase of the solution concentration across the line will cause that the hydrate (solid) can form as it is thermodynamically more stable than the solution. Right: pH map in the calcium alumina plane.

The arrows indicates the direction of the pore solution change during the hypothetical congruent dissolution. The doted lines are showing the evolution of the solution during the hypothetical congruent dissolution of CA and C12A7 phases. For this simulation, low S concentration of 0.0001 mM and K equal to 1 mM was used.

141

142   **3.2. Effect of sulphur and alkali on the solubility relationships in the Ca – Al – H₂O system**

143   In principle, this kind of graph and analysis can also be used for the examination of the hydration of ye'elimite

144   since it enables the solubility lines of the hydrates involved including ettringite (Et), monosulfate (MS),

145   aluminium hydroxide (AH_3), CAH_{10}, $C_2AH_{7.5}$, C_3AH_6 and C_4AH_{13}, to be plotted at any sulphur concentration.

146   However, this type of graph cannot be used to visualise varying sulphur concentrations or the effect of alkalis.

147   The dissolving ye'elimite releases three different elements into the solution: Ca, Al and sulphur. Their

148   speciation (Ca^{2+}; $CaOH^+$, …) changes depending on solution concentrations, which increase during the

149   dissolution of ye'elimite. The effect of sulphur concentration is intuitive for the ettringite and monosulfate

150   phases, since they contain sulphur. However, sulphur has an even more pronounced effect on other, sulfate-

free, phases because of the complex interactions within the pore solution as shown in Figure 2. Similarly, the presence of the alkalis in the system has an effect on the ion speciation, ionic strength of the solution and pH which modifies the solubility lines and surfaces calculated for a given scenario. In this section, both these effects are illustrated and discussed. Note that OH^- is not a free variable as its concentration is determined by the concentration of Ca, Al, S and alkalis, if present, and the global charge balance.

In Figure 2 the solubility lines in the Ca – Al plane are compared for two sulphur concentrations. The solubility lines of three hydrates important for the hydration of ye'elimite: aluminium hydroxide (amorphous and gibbsite), CAH_{10} and ettringite, are plotted in the calcium – alumina plane in Figure 2 for sulphur concentrations of 0.1 mM (solid lines) and 1 mM (dashed lines) . It is obvious that the sulphur concentrations influence the solubility lines of all hydrates:

- aluminium hydroxide (Figure 2 Left): the shape of the curves depends on the sulphur concentration for total Ca and Al concentration lower than 10 mM. It is noticeable that:

    o At lower sulphur concentration, the solubility of aluminium hydroxide increases with increasing Ca concentration as this increases the pH. At the higher sulphur concentration (which lowers the pH) the curves are not monotonic. Alumina solubility decreases with increasing calcium up to ~ 0.5 mM, while Ca concentrations > 0.5 mM solubilise aluminium hydroxide.

    o At the lower sulphur concentration, the amorphous form of aluminium hydroxide is always in equilibrium with much higher aluminium concentration than gibbsite. However, at S = 1 mM and lower Ca concentration, the difference in the aluminium concentration between the two forms becomes small.

    o At Ca and Al above 10 mM, the sulphur concentration has little impact on the solubility lines of either polymorph of aluminium hydroxide.

- Ettringite (Figure 2 Right): The increasing sulphur concentration results in a shift of the solubility line at lower calcium and aluminium concentrations, while at higher Al and Ca concentrations, the increasing S concentration results only in a slight increase of the ettringite solubility line. It is worth noticing, that the curved solubility lines of ettringite is in equilibrium with two different aluminium concentration at calcium

8

177   concentrations above 2 mM, which is counter intuitive; i.e. a vertical line at Ca concentration = 5mM

178   would cross the solubility line twice.

179   • The increasing sulphur concentration increases the solubility of the CAH10 (Figure 2 Right) phase in the

180   range of Ca concentrations 0.1 to ~ 3 mM. At the other Ca concentrations, the S concentration has limited

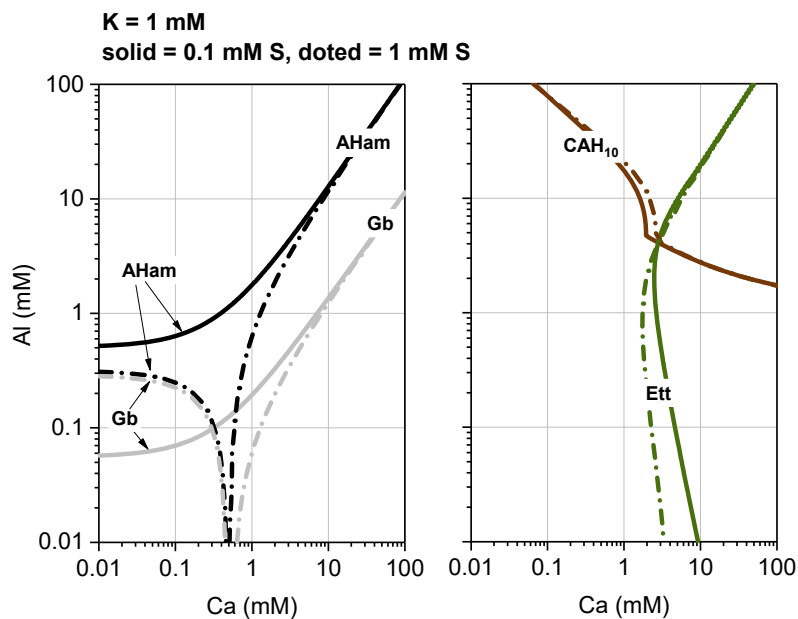181   impact (within the investigated range).

182

Figure 2 Solubility lines at different sulphur concentrations: CAH$_{10}$ - CAH$_{10}$ phase, Ett – Ettringite, Gb – gibbsite, AHam - aluminium hydroxide amorphous. The lines are showing the transition from liquid to solid. Increase of the solution concentration across the line will cause that the hydrate (solid) is more thermodynamically stable than the solution. The solid line shown the calculation results at 0.1 mM of S, and doted at 1 mM of S. K concentration is 1 mM for both cases.
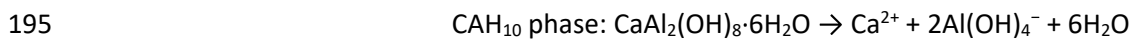
183

184   The evolutions observed have two explanations, depending on the chemical composition of the hydrates:

185   o   For the hydrates that do not contain sulphur (aluminium hydroxide and CAH$_{10}$), the influence of the

186   sulphur can be attributed

187   o   to the change in the ionic strength of the solution that directly impacts activity coefficients

188   of the ions involved in the solubility products;

189   o   to the complex formation between Ca^{2+} and SO_4^{2-} in solution and

190   o   to the lowering of OH^- concentration and consequently the decrease of the pore solution pH.

191   It should be noted that the OH^- is present in all the dissolution reactions and is coupled to pH via the

192   equilibrium reaction $H_2O \rightarrow OH^- + H^+$. For example the dissolution reactions of aluminium hydroxide and

193   CAH_{10} are at high pH as follows:

194   Aluminium hydroxide: $Al(OH)_3 + OH^- \rightarrow Al(OH)_4^-$

195   CAH_{10} phase: $CaAl_2(OH)_8 \cdot 6H_2O \rightarrow Ca^{2+} + 2Al(OH)_4^- + 6H_2O$

196   The evolution of the pH in the two investigated scenarios is shown in Figure 3: left shows the pH map

197   at the sulfate concentration of 0.1 mM and Figure 3-right at the sulfate concentration of 1 mM. The

198   dissolution of Aluminium hydroxide is amphoteric and the equilibrium aluminium concentrations

199   decrease strongly down to a pH of ~6.5 and then increases again at lower pH values. Figure 3 shows

200   how higher sulphur concentrations decrease the pH of the solution, in particular at low Ca and Al

201   concentrations. This decrease of solution pH strongly influences the solubility line of aluminium

202   hydroxide and explains the observed increase at very low Ca concentrations where the pH values

203   drop below 6. CAH_{10} shows much less dependence on the sulphur concentrations as for the higher

204   range of the Ca and Al concentrations pH is only moderately lowered.

205   o   For hydrates that contain sulphur, the effect is more complex. Sulphur impacts not only ionic

206   strength, complex formation and pH (OH^- concentration) but in addition the solubility product since

207   the sulphur takes part in the dissolution reaction as shown below for ettringite:

208   Ettringite: $Ca_6Al_2(SO_4)_3(OH)_{12} \cdot 26H_2O \rightarrow 6Ca^{2+} + 2Al(OH)_4^- + 3SO_4^{2-} + 4OH^- + 26H_2O$
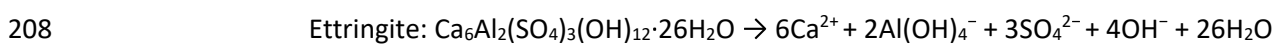
209   On the one hand, increasing sulphur concentrations will push the solubility lines to lower Ca and Al

210   concentrations because it is the part of the dissolution equation. On the other hand, increasing

211   sulphur concentration lowers the OH^- concentration, which would shift the solubility lines to higher
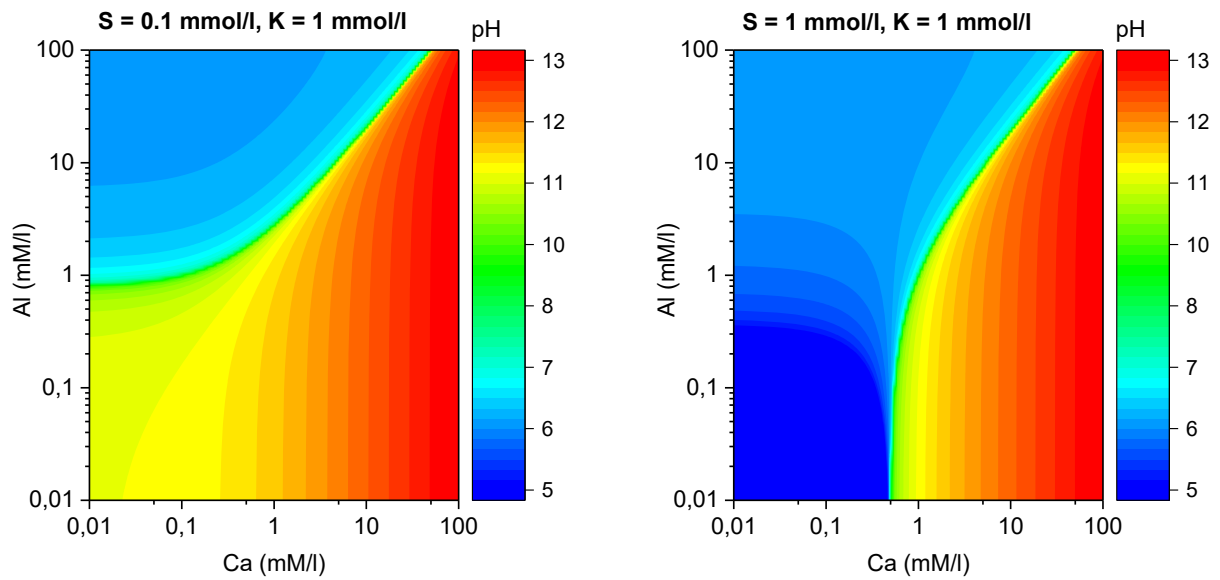
212   Ca and Al concentrations.

213

Figure 3 pH maps in the calcium alumina planes at the two sulphur levels 0.1 and 1 mM.

214

215   The effect of potassium on the solubility of the aluminium hydroxide, CAH_{10} phase and ettringite is shown in

216   Figure 4. Potassium increases both the ionic strength of the solution as well as its pH. This results in higher

217   aluminium concentrations in the presence of aluminium hydroxide and in a shift of the solubility line of

218   ettringite to lower Ca and Al concentrations. The effect on CAH_{10} is non monotonic. At lower Ca concentration

219   (< 3 mM), potassium lowers the Al concentrations. However, at high Ca concentrations (> 3 mM), more Al is
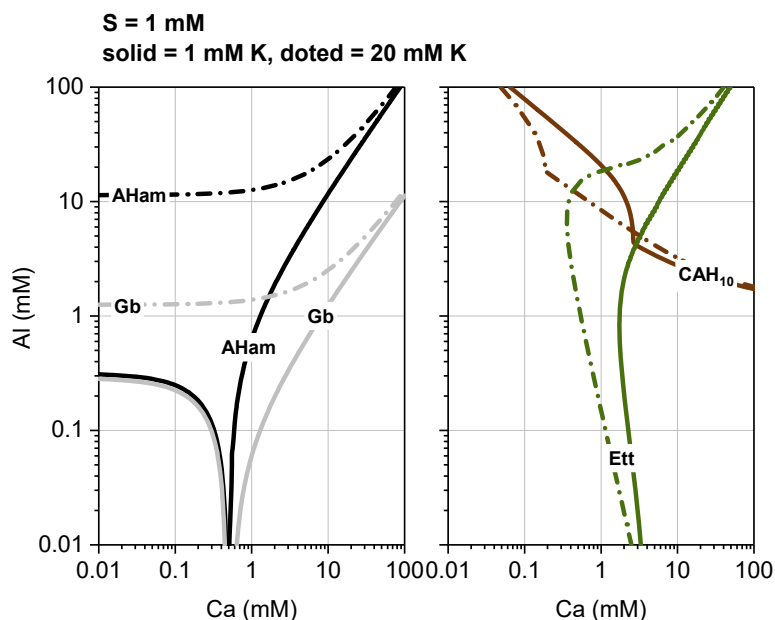
220   expected in the presence CAH_{10}.

221

S = 1 mM
solid = 1 mM K, doted = 20 mM K

Figure 4 Solubility lines at different K concentrations: CAH$_{10}$ - CAH$_{10}$ phase, Ett – Ettringite, Gb – gibbsite, AHam - aluminium hydroxide amorphous. The solid line shown the calculation results at 1 mM of K, and doted 20 mM of K. Sulphur concentration is 1 mM in both cases.

3.3. Three dimensional representation of the system

As shown above the interactions in the pore solution in the Ca-Al-S-K-H$_2$O system are complex as the sulphur and potassium have a strong impact on the ionic strength, on complex formation and the pH of the solution. These in turn significantly affect the solubility lines even of sulfate-free hydrates. Since the dissolution of ye'elimite provides Ca, Al and sulphur to the solution, the analysis of solubility lines plotted in 2-dimensions cannot capture the complexity of these systems and plots in 3-dimensions showing solubility surfaces instead of lines are better suited. The three-dimensional diagram of solubility surfaces in the systems Ca-Al-S-H$_2$O is shown in Figure 5 in the range of 0.01 to 100 mM Ca, Al and sulphur at K = 1 mM. The surfaces for the phases Ett, aluminium hydroxide (gibbsite), CAH$_{10}$, C$_2$AH$_{7.5}$, and C$_4$AH$_{13}$ are shown as well as the theoretical dissolution line of stoichiometric ye'elimite. It is noticeable that solubility surfaces of Ett, C$_2$AH$_{7.5}$, and C$_4$AH$_{13}$ are close to each other (note however the logarithmic scale) and their mutual distance as well as their crossings vary depending on the concentrations in the pore solution. Note that the solubility surface of monosulfate closely follows that of ettringite in the scenario modelled. The solubility surfaces of the remaining two hydrates, aluminium hydroxide and CAH$_{10}$, are distinctly different. While CAH$_{10}$ is

236 supersaturated only for high Al concentrations irrespective of those of calcium and sulphur, the solutions will

237 be supersaturated with respect to aluminium hydroxide for practically any concentration, except at very high

238 sulphur and calcium concentrations. Counter intuitively, the aluminium hydroxide solubility surface is the

239 most complex one, inspite of there being no calcium of sulphur in aluminium hydroxide. The complex shape

240 of the surface is a result of the interactions in the pore solution and their impact on pH. Note that the

241 solubility surfaces of the different forms of aluminium hydroxide (amorphous, microcrystalline, crystalline)

242 have a similar shape and are only 'shifted' along the vertical axis with aluminium concentration

243 Additionally, Figure 5 shows that during the theoretical calculated dissolution of the ye'elimite in pure water,

244 the solution is oversaturated with respect to several hydrates in the order aluminium hydroxide, CAH_{10} and

245 ettringite. Finally, the solution becomes supersaturated with the respect to the remaining hydrates

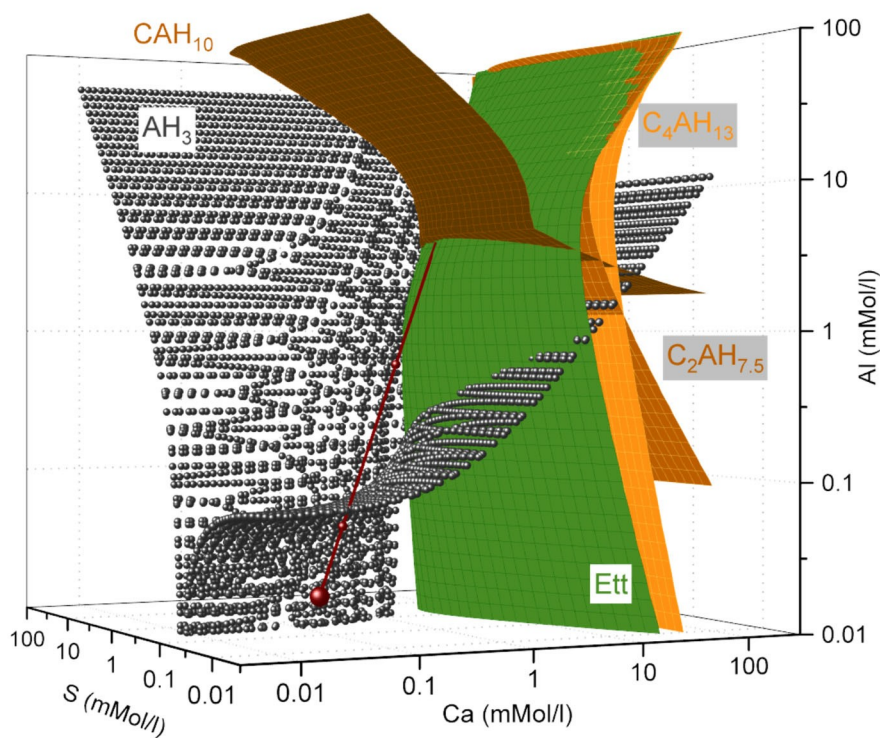246 investigated, if precipitation is not considered.

Figure 5 Solubility surfaces for the system Ca-Al-S-H$_2$O. K concentration is 1 mM. The red line shows the calculated change of the concentrations as a result of ye'elimite congruent dissolution.

247

248 So far, only generic results of the thermodynamic model have been considered and the complexity resulting

249 from the interactions in multi-species solutions of high ionic strengths discussed. The key messages are

250 following:

13

251   • Hydration reactions in Ca-Al-S-K-H$_2$O system cannot be analysed based on total concentrations and

252   a model accounting for speciation at high ionic strength is necessary.

253   • Solubility surfaces of phases are complex and highly dependent on activities of all ions including those

254   not involved in the solubility product equation.

255 At the initial stage of hydration, some phases such as aluminium hydroxide are very sensitive to even small

256 changes in alkali or sulphur concentrations.

257   **3.4. Reaction of ye'elimite in pure water**

258 In this section, the dissolution of ye'elimite is considered in detail to identify the stable hydrate domains and

259 how these are affected by the changing Ca, Al and sulphur concentrations. In addition, the relation between

260 the solubility surfaces and the evolution of the measured pore solution concentrations during the hydration

261 of ye'elimite are discussed. At the beginning of this section, the hydration of the pure ye'elimite is presented

262 shortly, based on earlier publication [9].

263 Figure 7 shows the evolution of the phase assemblage during the hydration of ye'elimite focussing on early

264 age. In these experiments, pure lab-synthesized ye'elimite and pure water were used [9], such that very low

265 alkali concentration of lower than 1 mM was present. Initially, ye'elimite reacts slowly, particularly up to

266 about 200 minutes. During this period, the main hydration products are ettringite and an XRD amorphous

267 phase. The reaction of Ye'elimite accelerates at about 500 minutes, the main hydration products observed

268 are monosulfate and XRD amorphous phase. Ye'elimite is fully hydrated at about 700 minutes. More detailed

269 description of the hydration process of ye'elimite is summarised e.g. in [9] and further extended in [10].
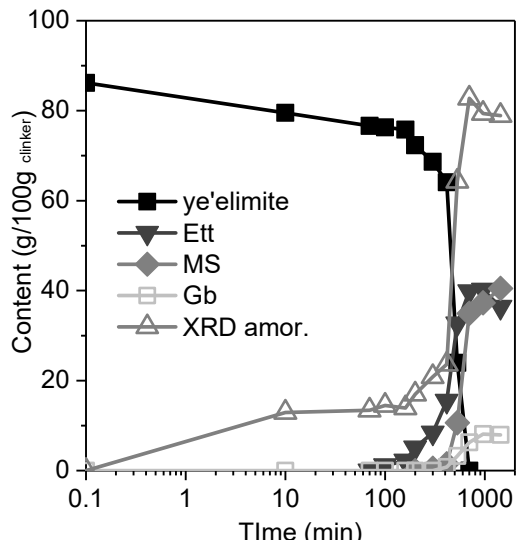
270

14

271

272 Figure 7 shows the measured concentrations in the pore solution and calculated saturation indexes. The Ca,

273 Al and sulphur concentrations increase in parallel up to about 90 minutes. During this period, little ye'elimite

274 reaction is observed. Between 90 minutes and 400 minutes, the solution changes with strongly increasing Al

275 concentration and a drop in sulphur. Finally, the concentrations decrease. The saturation indexes confirm

276 that the main hydration products are ettringite and monosulphate as described above when discussing XRD

277 data. Additionally, they suggest that the amorphous phase is composed of aluminium hydroxide and CAH_{10}
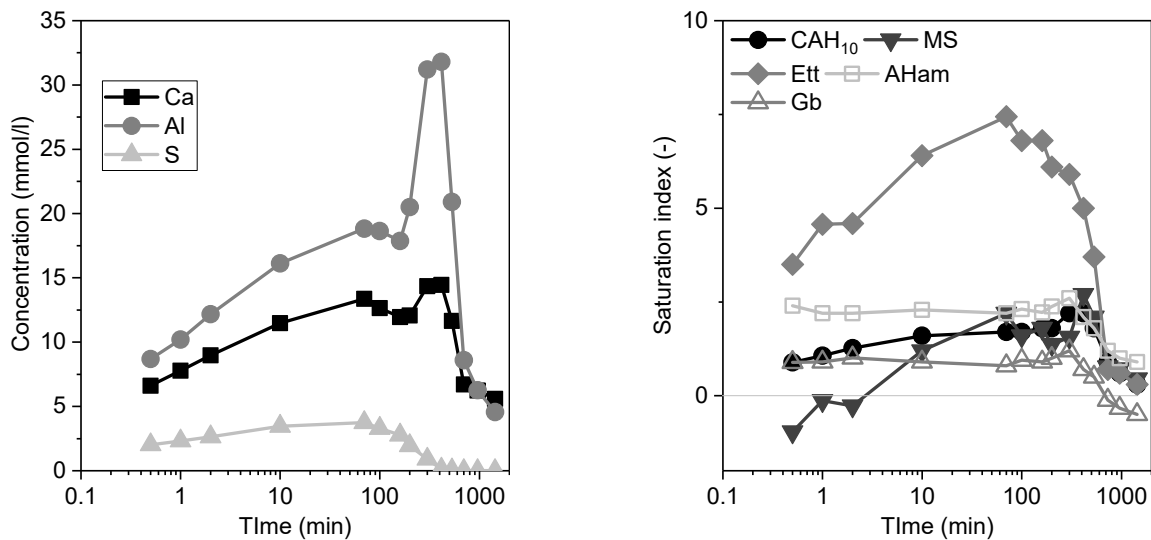
278 phase [9].

Figure 7 Pore solution concentrations measured during the reaction of ye'elimite at w/s = 40 in pure water.

Measured concentrations from [9]

15

279 In Figure 8 the measured pore solution concentrations from Figure 7 and [9] are compared with the

280 calculated solution concentration change during the pure dissolution of ye'elimite in pure water (indicated

281 by the red line) and the solubility surface of ettringite. The first measurements point (30 seconds) lies on the

282 calculated theoretical dissolution of ye'elimite indicating that the pore solution concentrations are changing

283 according to the theoretical dissolution line and no solids or a solid with a composition comparable to

284 ye'elimite have precipitated. The congruent dissolution path is followed up to about 90 minutes where

285 maximum solution concentrations of 15 mM Ca, 20 mM Al and 4 mM sulphur are reached.
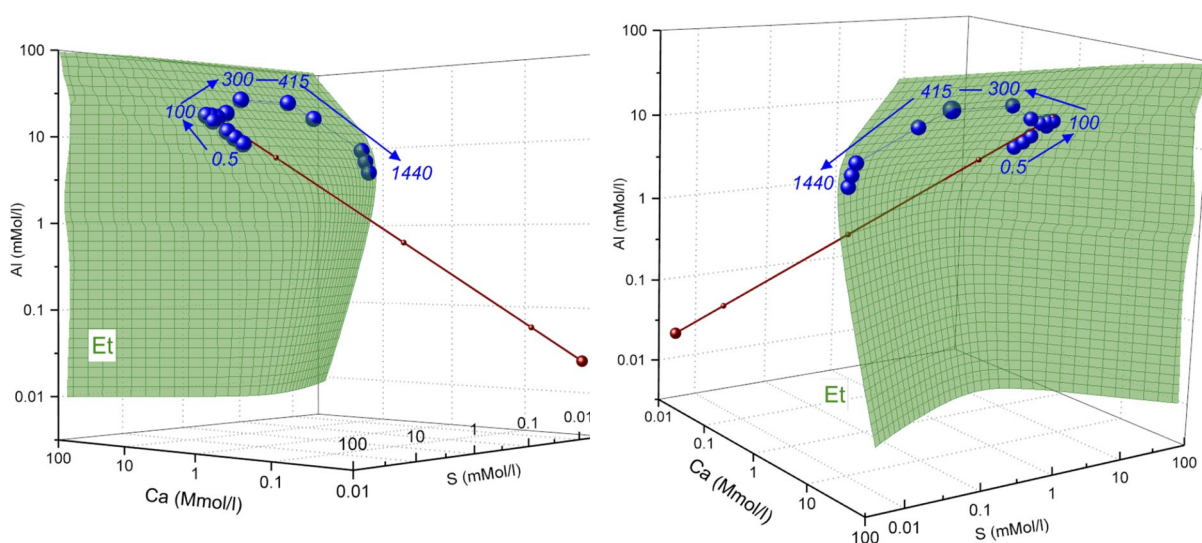
286

Figure 8 Solubility surface of ettringite calculated at 1 mM K compared to the theoretical dissolution line of ye'elimite (red) and measured concentrations of Ca, Al and S during the reaction of the synthetic, pure ye'elimite at w/c = 100 (blue points) [9]. The first measurement point is after 30 seconds. The arrows indicate the time evolution of the pore solution and the numbers the time of measurement in minutes. Both graphs show the same results but viewed from different perspective.

287

288 After 90 minutes, the concentrations deviate from the congruent dissolution line, indicating the formation

289 of a solid rich in calcium and sulfate. During the further reaction of ye'elimite, the measured pore solution

290 concentrations stay close to the surface of ettringite and other hydrates (Figure 8 and compare to [9]) .

291   While the 3 D-graphs allow all surfaces at to be plotted at the same time, the level of complexity in such

292   graphs is very high, consequently only intersections of surfaces from Figure 5 with different sulphur levels

293   are plotted in Figure 9 to facilitate the discussion of the results. Additionally, the 2 D-graphs show all three
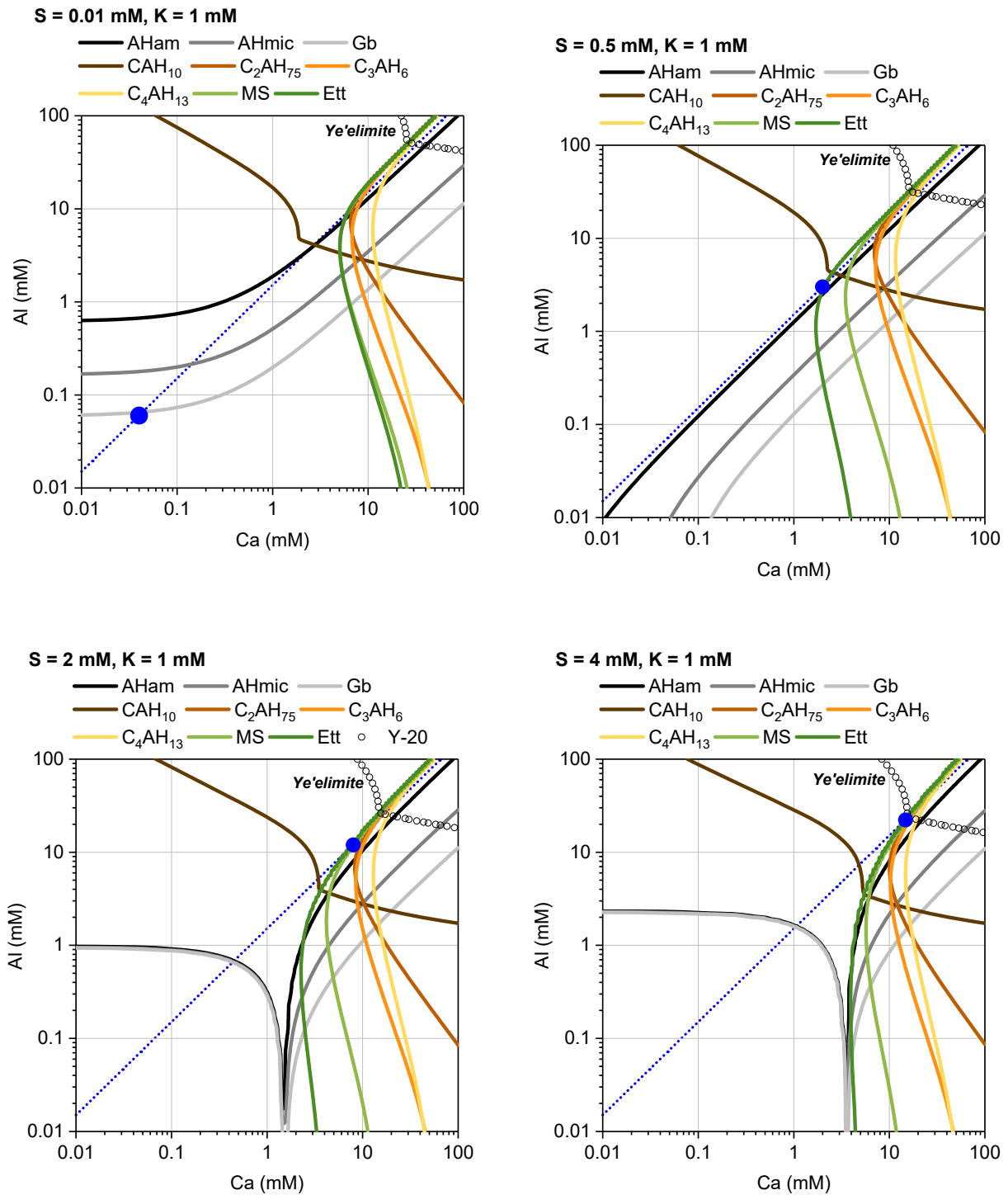
294   crystallinities of aluminium hydroxide.

295

Figure 9 Intersections of surfaces from Figure 5 at different sulphur concentrations: CAH_{10}, $C_2AH_{7.5}$, C_3AH_6 , C_4AH_{13}, MS: monosulfate, Ett: Ettringite, Gb: gibbsite, AHmic – aluminium hydroxide microcrystalline, AHam - aluminium hydroxide amorphous. The straight dotted line shows the projection of theoretical congruent dissolution line of ye'elimite on the Ca – Al plane. The blue circles depict the Ca and Al concentration corresponding to the concentration of S marked in the graph description. The plot at S = 2 mM corresponds to the first measurement point at 30 s from hydration starting. The plot at S = 4 mM corresponds to the point after ~90 minutes of the hydration. The ye'elimite line (Y-20) depicts solubility of ye'elimite decreased for 20 log units.

296

297   For the congruent dissolution of ye'elimite , the concentrations of Al, Ca and S should increase continuously

298   as visualised by the blue dotted line in Figure 9, S = 0.01 to 4 mM, until solids start to precipitate. This

299   theoretical dissolution line first crosses the solubility line of gibbsite; however, the precipitation of this

300   crystalline phase is very slow at ambient temperature, so rather amorphous or microcrystalline aluminium

301   hydroxide forms [18]. The solubility lines of the microcrystalline and amorphous forms of aluminium

302   hydroxide would be crossed at very low sulphur concentrations. However, in parallel to the Al and Ca

303   concentration, also the sulphur concentration increases, which lowers the pH values and changes the

304   solubility lines of aluminium hydroxide as had been discussed above for Figure 2. Thus, the further increase

305   of the solution concentrations does not result in significant increases in supersaturation with respect to

306   amorphous aluminium hydroxide (Figure 9 S = 0.5, 1 and 4 mM) as the slope of the surface of AHam is similar

307   to the dissolution curve of ye'elimite at sulphur concentrations larger than ~0.5 mM. At later times of

308   dissolution, i.e. at sulphur concentrations above 0.5 mM, the theoretical dissolution line of ye'elimite crosses

309   the solubility line of ettringite followed by CAH_{10} phase. Further dissolution of ye'elimite results in continuous

310   increases of the supersaturation against the CAH_{10} phase. However, the supersaturation with respect to

311   ettringite is limited because of the shape of its solubility surface almost parallel with the dissolution line

312   (compare with calculated SI in Figure 6). The experiments with a pure ye'elimite ([9], Figure 7 and Figure 6)

313   demonstrate that the solution composition follows, after the first 90 minutes, the trend of the solubility

314   surface of ettringite, as also mirrored in the only moderate oversaturation of ettringite. Finally, it is noticeable

315   that during the first minutes of ye'elimite dissolution, the undersaturation with respect to monosulfate

18

continuously increases. Only at the intermediate stages (after ~ 400 minutes) of the dissolution reaction when the elements concentrations increase, monosulfate becomes oversaturated (corresponding to sulphur concentration close to 4 mM). Gypsum is continuously undersaturated for all concentrations studied.

The shape of the solubility surfaces of the main hydrates is such that the continuous increase of the Al, Ca and sulphur results in a relatively small increase of the supersaturation against the main hydrated phases and thus in a relatively slow nucleation and precipitation, which explains the slow initial reaction of the synthetic neat ye'elimite observed by calorimetry [9].

This low oversaturation occurs because gibbsite does not precipitate fast enough and only the amorphous form of aluminium hydroxide precipitates to small extend during the first hours of ye'elimite reaction [9]. A massive precipitation of gibbsite would deplete Al from the solution and the dissolution line would follow the gibbsite surface instead of the congruent dissolution line in Figure 9. In such a case, the saturation surfaces of ettringite and monosulfate would be crossed sooner (see Figure 9 at S = 2 and 4 mM) such that the supersaturation with respect to ettringite and monosulfate would increase more rapidly leading to earlier and more intense nucleation and precipitation of these two phases. A significant precipitation of CAH_{10} (Figure 9, S = 2 and 4 mM) would have a similar effect, though less pronounced, and would lead to an earlier nucleation and precipitation compared to the stoichiometric ye'elimite dissolution. In fact, the plot of the experimental data and the congruent solubility curve illustrates that a small quantity of aluminium rich-hydrates has precipitated [9] during the early hydration as shown in Figure 10. This lowers the aluminium concentrations and results in a faster increase of the supersaturation which respect to the ettringite and later on monosulfate than if no phase had precipitated.
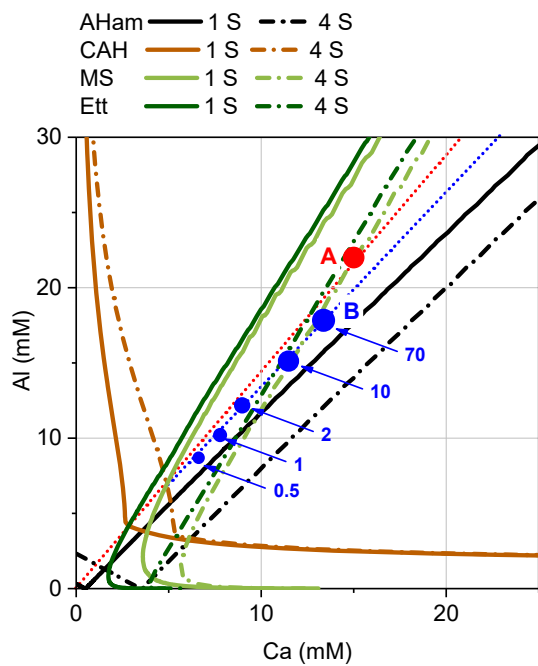
Figure 10 Intersections of surfaces of CAH - CAH_{10}, MS – monosulfate, Ett – Ettringite, and AHam - aluminium hydroxide amorphous at 1 and 4 mM sulphur concentrations. The straight red dotted line shows the projection of theoretical dissolution line of ye'elimite on the Ca – Al plane. The blue points show the measured pore solution centration evolution during the first 70 minutes (numbers gives the measurement time). Point B shown the measured concentrations rat the highest sulphur level (~ 4 mM S) while point A represents the theoretical Ca and Al concentration assuming no precipitation.

337 Figure 11 shows the evolution of the measured pore solution concentrations between 90 minutes and 700

338 minutes of hydration at w/b = 40. It is noticeable that the increase of the alumina concentration at the end

339 of the dormant period is related to two phenomena:

340 • Hydrates precipitation leads to the accumulation of the alumina in pore solution, indicating the

341   slower precipitation of AHam already discussed

342 • The decrease of the sulphur concentration increases the pH of the pore solution and the shape of

343   the solubility surface such that monosulfate and ettringite continue to be supersaturated

344 • This increase of pH leads also to a change of the aluminium hydroxide solubility surfaces, such that

345   after longer time the amorphous aluminium hydroxide becomes undersaturated and microcrystalline

346   aluminium hydroxide starts to form (in agreement with occurrence of a more crystalline aluminium
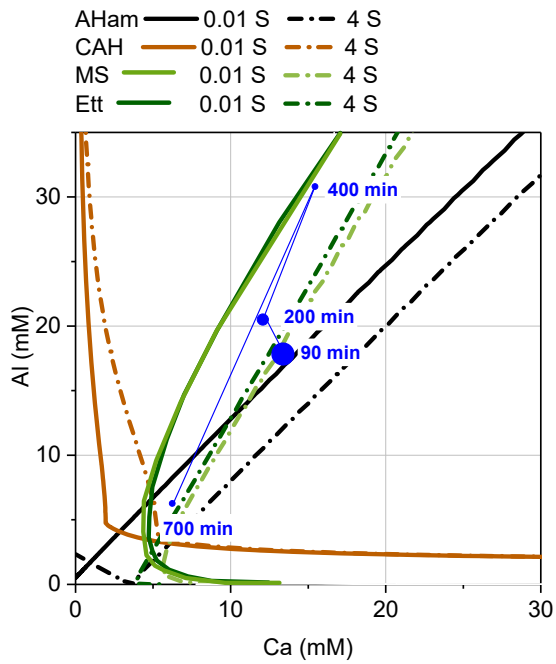
347   hydroxide as shown in Figure 7)

348

Figure 11 Intersections of surfaces of CAH - CAH$_{10}$, MS – monosulfate, Ett – Ettringite, and AHam - aluminium hydroxide amorphous at 0.01 and 4 mM sulphur concentrations.

The blue points show the measured pore solution centration evolution during the measurement after 90 minutes at the highest sulphur level (~ 4 mM sulphur). The other points represent the measured data after 200, 400 and 700 minutes and low sulphur concentrations (~ 0.01 mM sulphur after 700 min).

3.5. Towards industrial cement

Until now, we have focused on the dissolution of neat stoichiometric ye'elimite and the effects caused by

the interactions in the high ionic strength solution. Based on the changes to the saturation surfaces modelled,

the sequence of events in the dissolving and hydrating systems could be explained. Even in this simpler case,

the interactions were complex. Here we investigate in detail the dissolution of ye'elimite in the BYF clinker

and the impact of reacting rapidly phases like alkali sulphates and C$_{12}$A$_7$.

At the beginning of this section, the hydration of the BYF clinker is summarised, based on an earlier

publication [20]. The evolution of the phase assemblage at the beginning of the hydration of BYF cement is

dominated by the reaction of ye'elimite and principally similar to the pure ye'elimite as shown in Figure 12.

It is noticeable that the dormant period is significantly shorter: ye'elimite starts to rapidly react after about
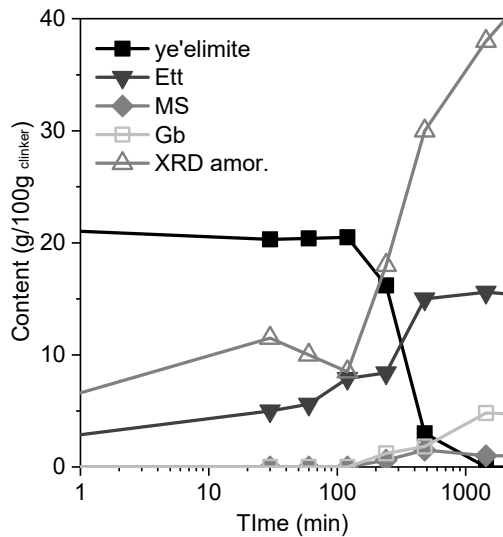
120 minutes of hydration.

Figure 12 Evolution of the content of selected phases during BYF clinker hydration at w/b =2. Data replotted from [20].

The pore solution evolution is shown in Figure 13. The evolution of the alumina concentration is similar to that of pure ye'elimite, but with significantly higher concentration values. The concentrations of calcium and sulphur are decreasing from the first measurement time, i.e. after 5 minutes from mixing with water. This indicates, in contrast to the pure ye'elimite system discussed above, precipitation of calcium and sulphur rich solids, consistent with the very early ettringite formation observed in these systems. Also, the sulphur concentrations are significantly higher than observed for the ye'elimite reacting in pure water (c.f. Figure 7). Additionally, the alkali concentration is high in industrial cements. The higher alkali concentration and high initial sulphur concentrations are related to the alkali sulphates typically present in industrial and semi industrial clinkers. Alkali sulphates dissolve almost instantly in mixing water leading to high alkali and sulphur concentrations.
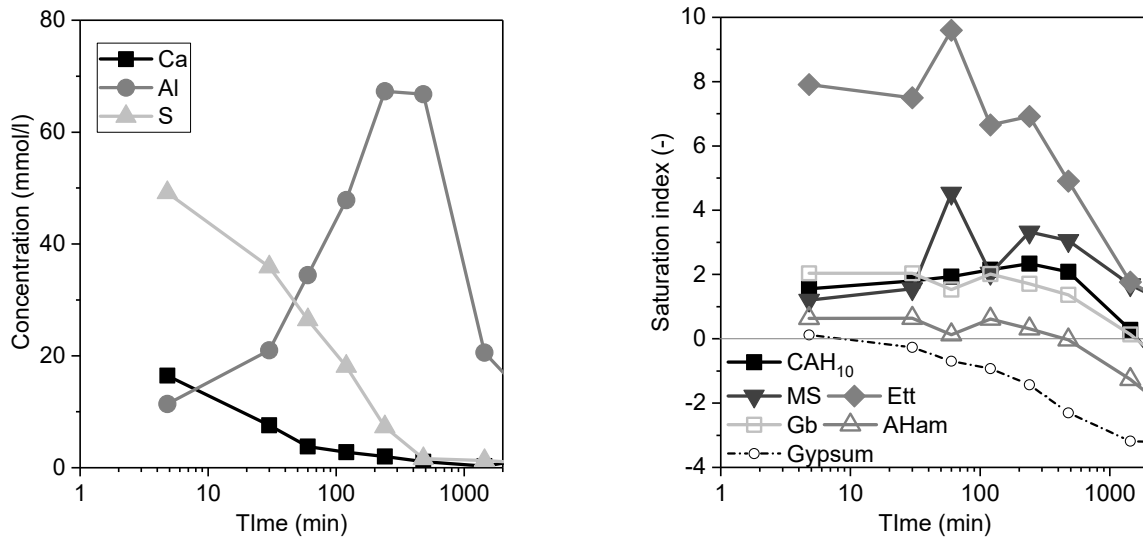
Figure 13 Pore solution concentrations measured during the reaction of BYF clinker at w/s = 2 in pure water. Measured concentrations from [9].

374   These differences are also related to the presence of minor phases that are formed during the clinkering

375   process and which significantly influence the hydration of ye'elimite in the cement. Calcium aluminate

376   phases, CA and $C_{12}A_7$, are often present in laboratory and industrial clinkers [12][13][14][44][45][46].

377   Particularly $C_{12}A_7$ reacts rapidly during the first minutes of the cement hydration [20][45][46] and has been

378   shown to accelerate the kinetics of the ye'elimite hydration [10].

379

380   The effect of the presence of these phases on the dissolution process is explored in Figure 14 by plotting the

381   pore solution composition against the solubility surfaces. The solubility surfaces are calculated for alkali and

382   sulphur concentrations corresponding to data in Figure 13. In this work, the total alkali concentration at the

383   first measurement time was about 100 mM and this corresponds to a sulphur concentration of 50 mM

384   assuming they originate from readily soluble alkali sulphates. In order to simplify the analysis, we assumed

385   that potassium is the only alkali present and that its content does not change during the early age hydration

386   investigated. Again, the theoretical congruent dissolution curve of ye'elimite is plotted against the cross-

387   section of the solubility surfaces of the main hydrates at the different sulphur levels is shown in Figure 14.

388   The theoretical dissolution line of $C_{12}A_7$ phase has been added (red dotted line). This $C_{12}A_7$ dissolution line

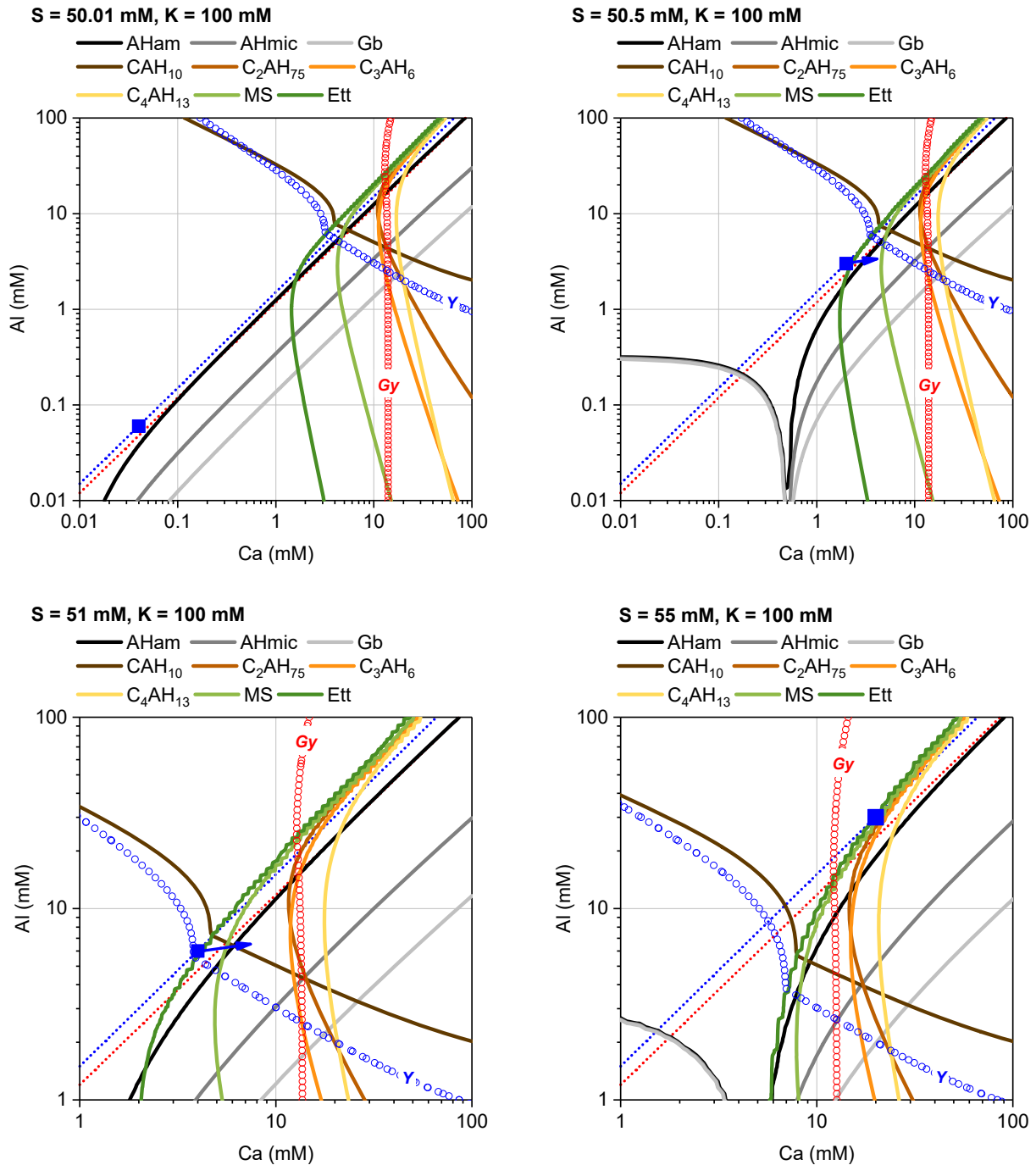389   runs nearly parallel to the ye'elimite dissolution line.

Figure 14 Intersections of solubility surfaces at different sulphur concentrations: Gy is the solubility surface of gypsum and Y is the ye'elimite solubility surface moved for 20 log units. In the calculation, an initial concentration of 50 mM K₂SO₄ was assumed.

The straight blue dotted line shows the theoretical congruent dissolution line of ye'elimite. The square blue points depict the Ca and Al concentration corresponding to the concentration of sulphur indicated on the graph. The straight red dotted line shows the Ca/Al ratio corresponding to the congruent, hypothetical dissolution of $C_{12}A_7$ phase. The arrow indicates the effect of $C_{12}A_7$ on the dissolution of ye'elimite.

390 The calculations reveals that the presence of 50 mM of K_2SO_4 in the solution (Figure 14) has a limited impact

391 on the calculated shape of the solubility surfaces of the calcium alumina hydrates compared to the case of

392 the dissolution of ye'elimite in pure water. The addition of only K_2SO_4 does not change the pH values

393 significantly when compare to the pure water (data not shown here). Only when more sulphur is added (so

394 the S/K is increased), which lowers the pH values, the curves show similar shifts as observed in Figure 9; thus

395 the concentration of sulphur of 0.01 mM in pure water corresponds to concentration of sulphur of 50.01 mM

396 in K_2SO_4 solution and 0.5 mM corresponds to 50.5 mM and so on.

397 There are two noticeable changes between the calculated solubility data for the pure water case and the

398 K_2SO_4 solution:

399   o Gypsum becomes supersaturated at higher calcium concentration for the case with K_2SO_4 in solution.

400   Note that in the Figure 9 gypsum was always under-saturated.

401   o At each investigated sulphur level, ye'elimite is less under saturated when compared to the

402   dissolution of the ye'elimite in the water.

403 The K_2SO_4 addition has a limited impact on the solubility lines of calcium alumina hydrates. Since the under-

404 saturation with respect to ye'elimite is lower at each sulphur level when compared to pure water case, its

405 reaction should be slower. However, the experiments provided in the literature show that ye'elimite reacts

406 significantly faster in the industrial cements; compare the kinetics of ye'elimite dissolution in Figure 6 and

407 Figure 12. The main reason for this acceleration is the $C_{12}A_7$ phase [10]. This phase has two pronounced

408 impacts on the calculated evolution of the pore solution during the dissolution of ye'elimite:

409   o The dissolution of $C_{12}A_7$ increases the Al and Ca concentration relative to the sulphur released from

410   ye'elimite.

411   o It moves the dissolution curve of the ye'elimite towards lower aluminium and higher calcium

412   concentrations as shown by the red dotted line in Figure 14,

413 These specific effects are confirmed by the pore solution concentrations measured during the dissolution of

414 ye'elimite in the presence on $C_{12}A_7$ as discussed in detail in [10]. These phenomena have a pronounced

415 impact on the development of the pore solution concentration relative to the solubility surfaces during the

416   dissolution ye'elimite in the cement clinker. At any given quantity of the ye'elimite dissolved, i.e. at the given

417   increase of the sulphur concentration in Figure 14, the solution is always more supersaturated initially with

418   respect to aluminium hydroxide and later on with respect to ettringite and CAH_{10}. Hence these phases can

419   precipitate earlier and faster. It is also noticeable that the presence of $C_{12}A_7$ results in a different order in

420   which the solubility surfaces are crossed during the ye'elimite dissolution. While in the case of pure ye'elimite

421   (Figure 9), the solution is supersaturated with respect to aluminium hydroxide and later on with respect to

422   CAH_{10} and ettringite, the presence of $C_{12}A_7$ and alkali sulfates in industrial clinkers modifies the pore solution

423   composition such that it is first supersaturated with respect to ettringite and later on with respect to CAH_{10}.

424   Overall, these changes contribute to the acceleration of ye'elimite hydration in the industrial cements

425   compared to the reaction of neat ye'elimite in pure water.

426   Another interesting point is the effect of alkalis on the evolution described above. The alkalis present as alkali

427   sulphate and those dissolved in the rapidly hydrating clinker phases (e.g. ye'elimite [27]) dissolve rapidly

428   during the first minutes of the cement hydration, which increases the pH of the pore solution and affects the

429   shape of the solubility surfaces. It should be noted that in the semi industrial and industrial cements the pH

430   of the pore solution is about 1 unit higher at all stages of the hydration than in the synthetic ye'elimite

431   dissolving in water (compare the data in [9], [10], [20], [25]). The effect of the alkali dissolution is shown in

432   Figure 15 for two S concentrations of 50.5 and 55 mM, respectively.
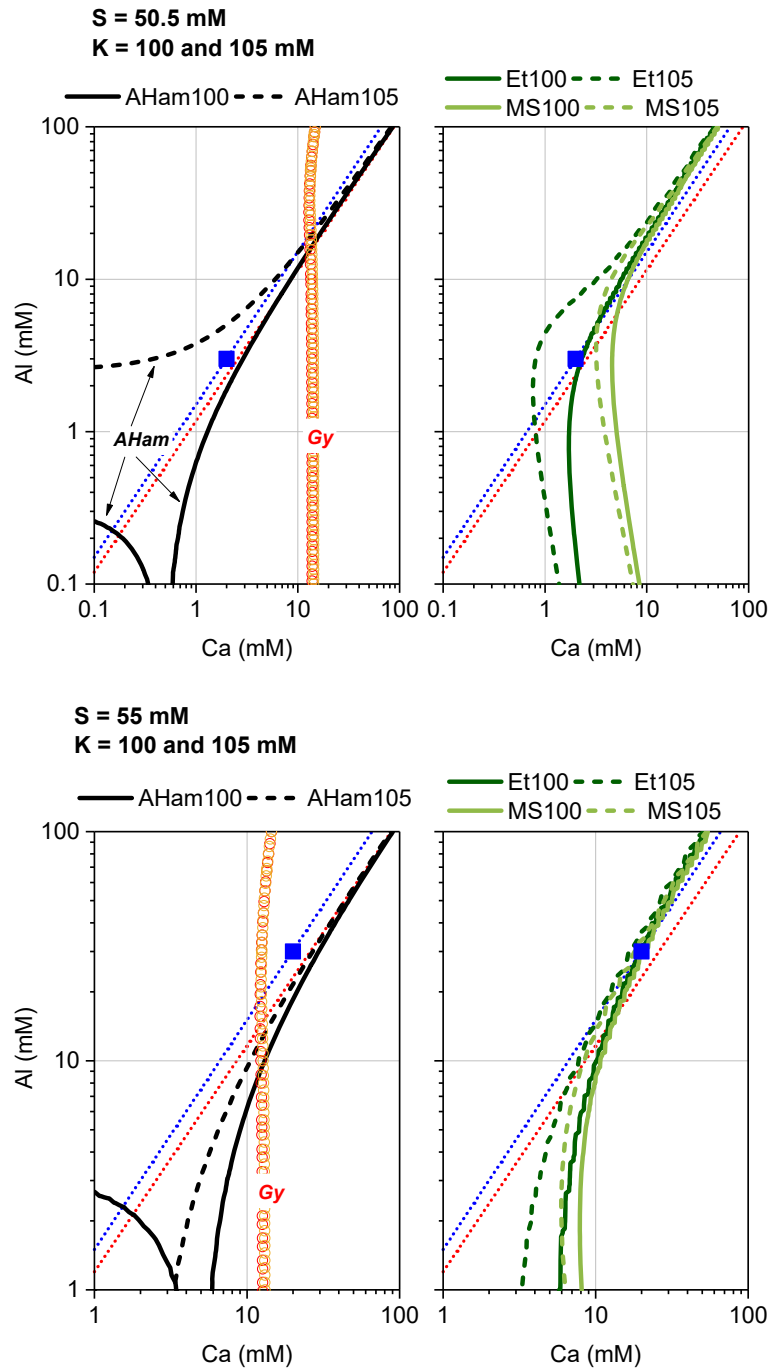
433

Figure 15 Intersections of solubility surfaces at S = 50.5 and 55 mM and two K concentrations equal to 100 and 105 mM. The straight blue dotted line shows the projection of theoretical dissolution line of ye'elimite on the Ca – Al plane. The square blue points depict the Ca and Al concentration corresponding to S = 0.5 at 1 mM from ye'elimite. The straight red dotted line shows the Ca/Al ratio corresponding to the dissolving $C_{12}A_7$ phase.

434

435   For this comparison the solubility surfaces were calculated at the alkali level K = 105 mM and compared to

436   the 100 mM as shown in Figure 15. It is noticeable that the increasing alkali concentration modifies the shape

437 of the solubility of ettringite and monosulfate in such way that they are crossed earlier and the

438 supersaturation increases more rapidly during the calculated dissolution of ye'elimite. Contrary, the solubility

439 surface of aluminium hydroxide is modified in the way that the solution is initially undersaturated with

440 respect to this phase at the higher alkali level. This can further contribute to the acceleration of the ye'elimite

441 hydration in industrial cement when compared to the pure ye'elimite reaction. It is important to notice that

442 the solubility surface of the gypsum is not significantly modified.

443 **4. Conclusions**

444 Thermodynamic modelling is a powerful tool to determine the variation of the system in presence of

445 solutions having known compositions. A knowledge of the equilibrium diagram is important even if the

446 system is dynamic (not at equilibrium) as occurs at the beginning of hydration: in fact it enables the kinetic

447 path of the reaction to be traced and so to determine if the solution is supersaturated or undersaturated

448 with respect to stable (or metastable hydrates if the metastable system is calculated) as mention already in

449 the 90s by Damidot and Glasser [30], [31] [32].

450 Contrary to previous studies on CAC and calcium silicates – the speciation model for high ionic strength

451 solutions enabled us to study the Ca-Al-S-K-H_2O system accounting for complex interactions in the pore

452 solution. By comparing the solubility surfaces with experimentally determined pore solution concentrations,

453 it is demonstrated that the hydration pathways follow the stability fields of certain hydrates.

454 For hydration of stoichiometric synthetic ye'elimite, the evolution of the pore solution concentrations

455 observed could be explained. During the initial dormant period, the saturation with respect to calcium

456 bearing hydrates changes significantly less than the changes of the concentrations would suggest. This is

457 caused by the interactions among the sulphur-bearing ionic species with alumina and calcium-bearing ones,

458 making the saturation surfaces almost parallel to the congruent dissolution line of ye'elimite. Once hydrates

459 start to precipitate, their supersaturation does not change as dramatically as the pore solution concentration.

460 Again, this is caused by the specific impact of the pore solution composition on the solubility of the involved

461 phases.

The same framework was successfully applied to the early hydration of industrial calcium sulfo-aluminates cements and shows how the presence of alkalis and C12A7 can accelerate the kinetics of ye'elimite hydration. While the alkalis from soluble salts such as $(Na,K)SO_4$ have little impact on the hydration path, alkalis dissolved in clinker forming phases move the solubility surfaces of the hydrated phases towards lower concentrations of Ca, Al and sulphur which accelerates the hydration process. A similar impact could be associated with the presence and dissolution of $C_{12}A_7$ from clinker.

The qualitative as well as quantitative agreement of the modelling results with the experimental data and observations not only proves the applicability of thermodynamic modelling to assessment of the hydration of calcium sulfo-aluminates, but also enables identification of the mechanisms involved which leads, finally, to a predictive model for the hydration pathways depending on the initial conditions and material compositions.

5. References

[1] F. P. Glasser and L. Zhang, "High-performance cement matrices based on calcium sulfoaluminate–belite compositions," *Cement and Concrete Research*, vol. 31, no. 12, pp. 1881–1886, 2001.

[2] M. C. G. Juenger, F. Winnefeld, J. L. Provis, and J. H. Ideker, "Advances in alternative cementitious binders," *Cement and Concrete Research*, vol. 41, no. 12, pp. 1232–1243, Dec. 2011.

[3] T. Sui, "Progress and future perspectives of CSA cements in China," in *International Workshop on Calcium Sulfoaluminate cements*, Murten, Switzerland, 2018.

[4] E. M. Gartner and D. E. Macphee, "A physico-chemical basis for novel cementitious binders," *Cement and Concrete Research*, vol. 41, no. 7, pp. 736–749, Jul. 2011.

[5] E. Gartner and H. Hirao, "A review of alternative approaches to the reduction of CO2 emissions associated with the manufacture of the binder phase in concrete," *Cement and Concrete Research*, vol. 78, pp. 126–142, Dec. 2015.

[6] W. Dienemann, D. Schmitt, F. Bullerjahn, and M. B. Haha, "Belite-Calciumsulfoaluminate-Ternesite (BCT)-a new low carbon clinker technology," *Cement International*, vol. 11, no. 4, pp. 100–109, 2013.

[7] J. Skocek, M. Zajac, B. Bullerjahn, and M. Ben Haha, "Effect of retarders on the early performance of CSA-type cement," *19th Ibausil. Weimar, Germany*, 2015.

[8] M. Zajac, J. Skocek, C. Stabler, F. Bullerjahn, and M. Ben Haha, "Hydration and performance evolution of belite–ye'elimite–ferrite cement," *Advances in Cement Research*, pp. 1–14, Sep. 2018.

[9] F. Bullerjahn, E. Boehm-Courjault, M. Zajac, M. Ben Haha, and K. Scrivener, "Hydration reactions and stages of clinker composed mainly of stoichiometric ye'elimite," *Cement and Concrete Research*, vol. 116, pp. 120–133, Feb. 2019.

[10] F. Bullerjahn, M. Zajac, M. Ben Haha, and K. L. Scrivener, "Factors influencing the hydration kinetics of ye'elimite; effect of mayenite," *Cement and Concrete Research*, vol. 116, pp. 113–119, Feb. 2019.

[11] F. Winnefeld and B. Lothenbach, "Phase equilibria in the system Ca 4 Al 6 O 12 SO 4–Ca 2 SiO 4–CaSO 4–H 2 O referring to the hydration of calcium sulfoaluminate cements," *RILEM Technical Letters*, vol. 1, pp. 10–16, 2016.

[12] S. Berger, C. Cau Dit Coumes, P. Le Bescop, and D. Damidot, "Hydration of calcium sulfoaluminate cement by a ZnCl 2 solution: Investigation at early age," *Cement and Concrete Research*, vol. 39, no. 12, pp. 1180–1187, Dec. 2009.

[13] S. Berger, C. C. D. Coumes, P. Le Bescop, and D. Damidot, "Influence of a thermal cycle at early age on the hydration of calcium sulphoaluminate cements with variable gypsum contents," *Cement and Concrete Research*, vol. 41, no. 2, pp. 149–160, Feb. 2011.

[14] P. Wang, N. Li, and L. Xu, "Hydration evolution and compressive strength of calcium sulphoaluminate cement constantly cured over the temperature range of 0 to 80 °C," *Cement and Concrete Research*, vol. 100, pp. 203–213, Oct. 2017.

[15] D. Gastaldi *et al.*, "Hydration products in sulfoaluminate cements: Evaluation of amorphous phases by XRD/solid-state NMR," *Cement and Concrete Research*, vol. 90, pp. 162–173, Dec. 2016.

[16] F. Song, Z. Yu, F. Yang, Y. Lu, and Y. Liu, "Microstructure of amorphous aluminum hydroxide in belite-calcium sulfoaluminate cement," *Cement and Concrete Research*, vol. 71, pp. 1–6, May 2015.

[17] Y. Zhang and J. Chang, "Microstructural evolution of aluminum hydroxide gel during the hydration of calcium sulfoaluminate under different alkali concentrations," *Construction and Building Materials*, vol. 180, pp. 655–664, Aug. 2018.

[18] B. Lothenbach, L. Pelletier-Chaignat, and F. Winnefeld, "Stability in the system CaO–Al2O3–H2O," *Cement and Concrete Research*, vol. 42, no. 12, pp. 1621–1634, Dec. 2012.

[19] D. Jansen, A. Spies, J. Neubauer, D. Ectors, and F. Goetz-Neunhoeffer, "Studies on the early hydration of two modifications of ye'elimite with gypsum," *Cement and Concrete Research*, vol. 91, pp. 106–116, 2017.

[20] M. Zajac, J. Skocek, F. Bullerjahn, and M. Ben Haha, "Effect of retarders on the early hydration of calcium-sulpho-aluminate (CSA) type cements," *Cement and Concrete Research*, vol. 84, pp. 62–75, Jun. 2016.

[21] V. Morin, P. Termkhajornkit, B. Huet, and G. Pham, "Impact of quantity of anhydrite, water to binder ratio, fineness on kinetics and phase assemblage of belite-ye'elimite-ferrite cement," *Cement and Concrete Research*, vol. 99, pp. 8–17, Sep. 2017.

[22] L. Zhang and F. P. Glasser, "Hydration of calcium sulfoaluminate cement at less than 24 h," *Advances in Cement Research*, Oct. 2002.

[23] J.-B. Champenois *et al.*, "Influence of sodium borate on the early age hydration of calcium sulfoaluminate cement," *Cement and Concrete Research*, vol. 70, pp. 83–93, Apr. 2015.

[24] C. Cau Dit Coumes, M. Dhoury, J.-B. Champenois, C. Mercier, and D. Damidot, "Combined effects of lithium and borate ions on the hydration of calcium sulfoaluminate cement," *Cement and Concrete Research*, vol. 97, pp. 50–60, Jul. 2017.

[25] F. Winnefeld and B. Lothenbach, "Hydration of calcium sulfoaluminate cements — Experimental findings and thermodynamic modelling," *Cement and Concrete Research*, vol. 40, no. 8, pp. 1239–1247, Aug. 2010.

[26] J. Wang, I. Baco, V. Morin, G. Walenta, D. Damidot, and E. Gartner, "Hydration mechanism of cements based on low-CO2 clinkers containing belite,ye_elimite and calcium.pdf," in *2010*, At Jinan, China, 2010, vol. Session 1.

[27] F. Bullerjahn, "Characterisation and hydration of ye'elimite containing cements," EPFL, 2018.

[28] K. L. Scrivener and A. Nonat, "Hydration of cementitious materials, present and future," *Cement and concrete research*, vol. 41, no. 7, pp. 651–665, 2011.

[29] D. Damidot, B. Lothenbach, D. Herfort, and F. P. Glasser, "Thermodynamics and cement science," *Cement and Concrete Research*, vol. 41, no. 7, pp. 679–695, Jul. 2011.

[30] D. Damidot and F. P. Glasser, "Thermodynamic investigation of the CaO-Al2O3-CaSO4-K2O-H2O system at 25° C," *Cement and concrete research*, vol. 23, no. 5, pp. 1195–1204, 1993.

[31] D. Damidot and F. P. Glasser, "Thermodynamic investigation of the CaO-Al2O3-CaSO4-H2O system at 25° C and the influence of Na2O," *Cement and Concrete Research*, vol. 23, no. 1, pp. 221–238, 1993.

[32] D. Damidot and F. Glasser, "Investigation of the CaO-Al2O3-SiO2-H2O system at 25 C by thermodynamic calculations," *Cement and Concrete Research*, vol. 25, no. 1, pp. 22–28, 1995.

550 [33] W. Hummel, U. Berner, E. Curti, F. Pearson, and T. Thoenen, "Nagra/PSI chemical thermodynamic data
551   base 01/01," *Radiochimica Acta*, vol. 90, no. 9-11/2002, pp. 805–813, 2002.
552 [34] W. Hummel, U. Berner, E. Curti, F. Pearson, and T. Thoenen, "Nagra Technical Report NTB 02-16,"
553   *Wettingen, Switzerland*, 2002.
554 [35] T. Matschei, B. Lothenbach, and F. P. Glasser, "Thermodynamic properties of Portland cement hydrates
555   in the system CaO–Al2O3–SiO2–CaSO4–CaCO3–H2O," *Cement and Concrete Research*, vol. 37, no. 10,
556   pp. 1379–1410, Oct. 2007.
557 [36] B. Lothenbach *et al.*, "Cemdata18: A thermodynamic database for hydrated Portland cements and
558   alkali-activated materials," *Cement and Concrete Research*, in press 2018.
559 [37] D. A. Kulik *et al.*, "GEM-Selektor geochemical modeling package: revised algorithm and GEMS3K
560   numerical kernel for coupled simulation codes," *Computational Geosciences*, vol. 17, no. 1, pp. 1–24,
561   2013.
562 [38] T. Wagner, D. A. Kulik, F. F. Hingerl, and S. V. Dmytrieva, "GEM-Selektor geochemical modeling package:
563   TSolMod library and data interface for multicomponent phase models," *The Canadian Mineralogist*,
564   vol. 50, no. 5, pp. 1173–1195, 2012.
565 [39] W. Wang, X. Chen, Y. Chen, Y. Dong, and C. Ma, "Calculation and verification for the thermodynamic
566   data of 3CaO· 3Al2O3· CaSO4," *Chinese Journal of Chemical Engineering*, vol. 19, no. 3, pp. 489–495,
567   2011.
568 [40] J. Wang, "Le mécanisme d'hydratation de ciment basé aux mâchefers Bas-CO2 contenant belite,
569   ye'elimite et l'alumino-ferrite de calcium," Université des Sciences et Technologie de Lille-Lille I, 2010.
570 [41] P. Barret, D. Bertrandie, and D. Beau, "Calcium hydrocarboaluminate, carbonate, alumina gel and
571   hydrated aluminates solubility diagram calculated in equilibrium with CO2g and with Naaq+ ions,"
572   *Cement and concrete research*, vol. 13, no. 6, pp. 789–800, 1983.
573 [42] F. M. Lea and P. C. Hewlett, *Lea's chemistry of cement and concrete*. Elsevier, 2004.
574 [43] G. Le Saout, "Calcium aluminate based hydraulic binders: a review," in *Conference: 2nd International
575   conference on the chemistry of construction materials,* Munisch, Germany, 2016, vol. 50.
576 [44] L. H. J. Martin, F. Winnefeld, E. Tschopp, C. J. Müller, and B. Lothenbach, "Influence of fly ash on the
577   hydration of calcium sulfoaluminate cement," *Cement and Concrete Research*, vol. 95, pp. 152–163,
578   May 2017.
579 [45] M. C. Martín-Sedeño *et al.*, "Aluminum-rich belite sulfoaluminate cements: Clinkering and early age
580   hydration," *Cement and Concrete Research*, vol. 40, no. 3, pp. 359–369, Mar. 2010.
581 [46] F. Bullerjahn, D. Schmitt, and M. Ben Haha, "Effect of raw mix design and of clinkering process on the
582   formation and mineralogical composition of (ternesite) belite calcium sulphoaluminate ferrite clinker,"
583   *Cement and Concrete Research*, vol. 59, pp. 87–95, May 2014.
584
585